Title: **Inverse determination of the fatigue Strain Energy Density control radius for conventionally and additively manufactured rounded V-notches**

Authors: **M. Benedetti, C. Santus, F. Berto**

DOI Link: https://doi.org/10.1016/j.ijfatigue.2019.04.040

Inverse determination of the fatigue Strain Energy Density control radius for conventionally and additively manufactured rounded V-notches

M. Benedetti[a], C. Santus[b,*], F. Berto[c]

[a]*Department of Industrial Engineering - DII, University of Trento, Italy.*
[b]*Department of Civil and Industrial Engineering - DICI, University of Pisa, Italy.*
[c]*Department of Mechanical and Industrial Engineering, NTNU - Norwegian University of Science and Technology, Trondheim, Norway.*

Abstract

The Strain Energy Density (SED) fatigue criterion is based on a material control radius. The value of this length is therefore required for an accurate assessment of the fatigue strength of any, especially severely, notched components. The singularity-based control radius is initially obtained by considering the hypothetical perfectly sharp V-notched specimen. The effect of the notch radius on the inverse search is then investigated with numerical simulations, and a new analytical procedure is introduced for the determination of the (actual) control radius. This procedure is applied to the experimental data of three metal alloys with different load ratios and manufacturing conditions.

Keywords: SED; control radius; inverse search; V-notched specimen; conventionally and additively manufactured alloys.

*Corresponding author: Ciro Santus
Ph. +39 (0)50 2218007
Email address: ciro.santus@ing.unipi.it (C. Santus)

Nomenclature

SED	Strain Energy Density
NSIF	Notch Stress Intensity Factor
FE	Finite Element (method)
SLM	Selective Laser Melting (additive manufacturing)
TCD	Theory of Critical Distances
LM	Line Method according to the TCD
2α	V-notch opening angle
D	Specimen bar diameter
A	Notch depth
R	Notch radius
R'	Dimensionless notch radius
r_0	Circular control area centre position
R_0	Mode I material-dependent control radius based on the singularity assumption
R'_0	Dimensionless mode I control radius based on the singularity assumption
R_1	Mode I material-dependent control radius
R'_1	Dimensionless mode I control radius
E	Young's modulus
ν	Poisson's ratio
s	Williams' power law singularity exponent
$\overline{W}_1$	Mode I SED
$\Delta\overline{W}_1$	SED associated with the fatigue full range
$\Delta\overline{W}_{1,\mathrm{plain}}$	SED associated with the fatigue full range of a mono-axial load
$\overline{W}_{1,\mathrm{maxref}}$	SED estimated with the maximum explored FE mesh refinement
e	Order of magnitude of the FE model element size
δ	Percentage relative deviation of the FE analysis
K_N	NSIF of the V-notched specimen
$K_{\mathrm{N,UU}}$	NSIF for unitary nominal stress and unitary half diameter
ΔK_th	Threshold stress intensity factor full range
$\Delta\sigma_\mathrm{fl}$	Plain specimen fatigue limit full range
σ_N	Notched specimen (net) nominal stress

$\Delta\sigma_{N,fl}$	Notched specimen nominal stress, fatigue limit full range
σ_a	Plain specimen stress amplitude
$\sigma_{N,a}$	Notched specimen (net) nominal stress amplitude
R	Fatigue load ratio
K_f	Fatigue stress concentration factor of the V-notched specimen
L	Critical distance
L_{th}	Threshold-based critical distance
$R_{1,th}$	Threshold-based control radius
$R'_{1,InvFun}$	Inverse search evaluation of the dimensionless control radius
$R'_{1,FE}$	FE evaluation of the dimensionless control radius
ε	Percentage relative difference between the FE and the inverse search control radii
$R'_{0,min}$	Minimum value allowed for R'_0
$K_{f,max}$	Maximum fatigue stress concentration factor
K_t	Stress concentration factor of the V-notched specimen
S	Sensitivity of the control radius inverse search
a_i, b_{ij}, c_k	Procedure coefficient arrays for the control radius inverse search
d_i, e_{ij}	Procedure coefficient arrays for the direct problem

1. Introduction

The concepts of "elementary volume" and "structural support length" were used for the first time by Neuber in his pioneering and illuminating works [1, 2]. The underlying idea is that the notch stress averaged over a short distance that is normal to the notch edge is the fatigue strength-effective parameter in the presence of sharp or point notches. Later on, Sheppard [3] proposed the idea that a quantity averaged over a finite size volume controls the fatigue behaviour of sharp notches by means of a single parameter, the average value of the circumferential $\sigma_{\theta\theta}$ stress. Since the first work by Beltrami [4], the Strain Energy Density (SED) has been employed to assess the static and fatigue behaviour of unnotched and notched components following many different SED-based approaches. Dealing with cracked components, and then notched components, the strain energy density factor S was defined by Sih [5] as the product of the strain energy density by a critical distance from the point of singularity. The failure was thought to be controlled by a critical value S_c, while the direction of the crack propagation was determined by imposing a minimum condition on S. Gillemot [6] calculated the deformation energy required for crack initiation in a unit volume of material, and extensively investigated the absorbed specific

fracture energy and its relationship with the critical value of J-integral and the critical value of S.

More recently, Lazzarin and Zambardi [7] proposed a strain energy density criterion stating that brittle failure occurs when the mean value of the strain energy density over a control volume (which becomes an area in two dimensional cases) is equal to a critical energy W_c. The SED approach as originally proposed, is based on the accurate definition of the control volume which is considered a material-dependent parameter. The radius of the control volume is a function of the ultimate tensile strength, the fracture toughness, and Poisson's ratio in the case of static loadings. Under cyclic loading, the critical radius similarly depends on the unnotched specimen fatigue limit, the threshold stress intensity factor range, and Poisson's ratio. This method was first formalized and applied to perfectly sharp (zero radius) V-notches, and a successful example was the application to welded joints proposed by Livieri and Lazzarin [8]. Welded specimens and structures with the weld bead geometry simplified just as the nominal 135° V-notch were also modelled by Fischer et al. [9, 10], again assuming a zero radius. In fact, this geometry feature is unreliable, and difficult to measure for weldments. Under this perfectly sharp (worst-case condition) hypothesis, the FE-based peak stress method can be efficiently applied and linked to the SED evaluation [11, 12]. The SED approach was then extended to blunt notches, and a thorough analytical approach that takes into account the effect of the notch radius was provided by Lazzarin and Berto [13]. A complete review of the volume-based SED approach including a final synthesis of more than 1900 experimental data from static and fatigue tests is reported in a review by Berto and Lazzarin [14]. Very different materials are considered with a control radius ranging from 0.4 μm to 500 μm.

The brittle fracture with U and V-notched specimens has been investigated by applying the SED criterion under mixed loading (in-plane) with different angles and local notch radius, showing the versatility of the method [15, 16, 17, 18, 19]. Multiaxial fatigue, including the mode III notch stress intensity factor, was also proposed and experimentally examined by Berto et al. [20, 21, 22]. One significant result was that the control radius was found to be dependent on the loading type under out of plane loading, thus two different critical radii were introduced, usually referred to as R_1 and R_3, for modes I and III respectively. However, Vantadori et al. [23] proposed the evaluation of a strain-based multiaxial LCF criterion at a unique verification point whose position is dependent on both R_1 and R_3.

From the above discussion, it is clear that a robust notch fatigue assessment necessitates an accurate determination of the material's characteristic control radius. Concerning the mode I type of loading, which is the only focus of the present paper, R_1 can be determined by imposing the SED equivalence of two different geometric configurations of fatigue loaded components [24, 25, 26]. Accordingly, in the original formulation of this approach, which is suitable for high-cycle fatigue strength prediction, it is assumed that a smooth sample under fatigue limit

$\Delta\sigma_{fl}$ loading and a cracked member under near-threshold ΔK_{th} condition show the same SED averaged over R_1. When both fatigue characteristics $\Delta\sigma_{fl}$ and ΔK_{th} are known, R_1 can be easily determined by imposing the aforementioned energy equivalence. However, this method has various shortcomings, already discussed in [27] and here briefly summarized: (i) though well documented in the ASTM standard [28], the determination of ΔK_{th} is experimentally challenging, especially with negative load ratios; (ii) this approach cannot be extended to the medium cycle fatigue regime as it is not clear which fracture mechanics parameter is representative of the crack growth resistance in the finite life regime.

To overcome these difficulties, the cracked specimen can be replaced with a notched specimen configuration, whereby the notch fatigue strength $\Delta\sigma_{N,fl}$ can be determined more easily and in a wide range of fatigue lives. Berto et al. [21, 29] and Radaj [11] determined R_1 using closed-form equations derived from the concept of the Notch Stress Intensity Factor (NSIF), i.e. based on the assumption of a perfectly sharp notch and stress field dominated by the singular term only. This approach needs to be modified when the non-singular stress terms significantly contribute to SED. This is especially true for a relatively large notch radius, for which the unavoidable deviation from the ideal sharp geometry perturbs the singular stress term, especially when R_1 is smaller than the local notch radius. The scenario is further complicated by the absence of a standardized procedure for R_1 determination, thus it is not clear which notched sample configuration is best for this purpose. Our research group recently tackled similar problem [27] by using an inverse search procedure for a robust determination of the critical distance length L necessary for fatigue calculations within the framework of the Theory of Critical Distances [30, 31, 32, 33]. This procedure is a development of the approach followed in [34, 35, 36, 37, 38, 39], as it is based on an optimized geometry of a rounded V-notched cylindrical specimen, wherein the notch depth is devised to maximize the intensity of the singular stress term. In this way, the resulting steep stress gradient at the notch tip makes the inverse search robust against the experimental uncertainty affecting the input of the method, i.e. the fatigue notch factor K_f. In our previous work [40], the role of the notch radius was extensively analysed, concluding that accurate L estimations, which are consistent with those derived from the crack threshold, are obtained if the notch is sharp enough, namely when the notch radius is in the order of 0.2 mm or less. However, an arbitrary small radius cannot be obtained, or at least is difficult to control. Therefore, the easiest and most reliable manufacturing method is to replicate the (turning) tool nose radius, simply by imposing a segmented trajectory to the tool and obtaining the minimum radius. More recently, we used the same optimal notch geometry in [41] to combine the TCD with several multiaxial fatigue criteria, and again the related critical distances were determined.

The present paper extends our methodology to a robust inverse search determination of the control radius R_1.

The procedure relies on a first approximation estimate of R_1 based on the NSIF singular stress field. This value is then corrected with an analytical procedure based on the interpolation of accurate numerical finite element simulations. In order to avoid too large a set of required coefficients, only the two main notch angles 60° and 90° are considered, combined with three Poisson's ratio values typical of metallic materials, i.e. 0.27, 0.3 and 0.33. MATLAB® functions for inverse and direct estimation of R_1 and K_f, respectively, are provided in the online version of the present article. The user of this method is thus not required to carry out FE calculations of the SED of the notched sample.

The analysis was performed on a dimensionless geometry, allowing an inverse search of a specimen of any size, and including a large range of ratios between the notch radius and the notch depth. The proposed procedure is applied to determine the control radius R_1 of two common structural materials, i.e. 42CrMo4 quenched and tempered (Q+T) steel and 7075-T6 aluminium alloy, and an additively manufactured Ti-6Al-4V alloy based on the fatigue experimentation carried out in two of our previous works [40] and [42], respectively. Finally, the method is validated by calculating the fatigue strength of a sample batch with a blunt notch and extended to the finite life regime.

2. Theoretical background

2.1. Notch and SED geometrical parameters

For the inverse search of the SED control radius, the V-notched cylindrical geometry is considered the most effective for the specimen, since it can be easily machined by turning, also with a small notch radius, and is not affected by any edge effects. The load applied to the specimen is axial, to induce a mode I loading on the notch, and the nominal stress parameter is defined as the uniform stress on the notch net area σ_N, Fig. 1 (a). A non-symmetrical notch, with the bisector not perpendicularly inclined to the specimen axis, would generate an additional mode II loading, thus potentially involving another material radius aimed at this load type [43]. Similarly, the torsion load would induce mode III and then R_3 would also be involved. However, in order to have a robust determination of R_1, only a pure mode I loading is pursued in this work.

The geometrical parameters are defined in Fig. 1 (a). Besides the notch opening angle 2α and the external diameter D, the specimen geometry is fully defined by the notch depth A and the notch radius R. The control radius R_1 is centred at a distance r_0 from the notch tip moving along the notch bisector, and r_0 is a function of both the notch radius R and the notch opening angle 2α[1]. The centre position of the control radius is $r_0 = 0.4\,R$ for $2\alpha = 60°$ and $r_0 = 0.333\,R$ for $2\alpha = 90°$ which are the only two angles considered in this study.

[1] In the present paper the notch opening angle is 2α, in agreement with the SED literature, while in our previous paper Santus et al. [27], the notch opening angle is α.

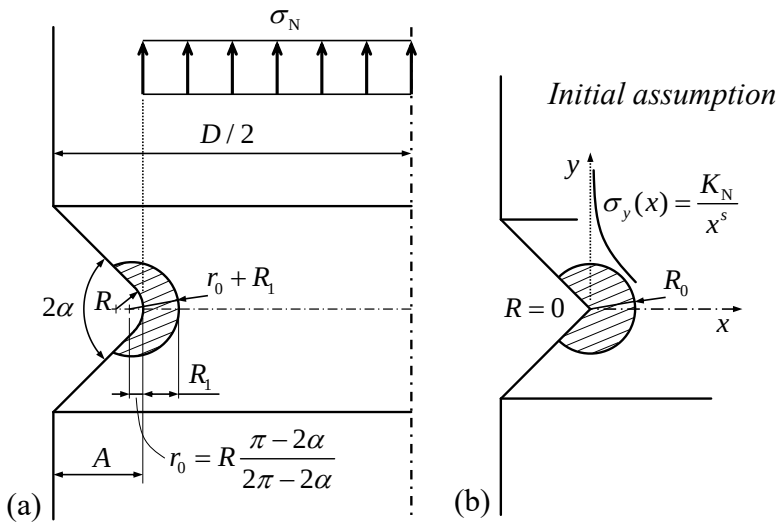

Figure 1: (a) V-notched specimen dimensions and material dependent size of the circular area where the strain energy is averaged. (b) Initial assumption based on singular stress distribution.

Without losing general validity of the results, the geometrical parameters are made non-dimensional by normalization with respect to the external radius $D/2$. The following analyses are limited to the special value of the non-dimensional notch depth $A/(D/2) = 0.3$, which was found in [27] to maximize the intensity of the singular stress term ahead of the notch tip. Once this size has been fixed along with the notch opening angle 2α (either 60° or 90°), the only remaining free geometrical parameter is the non-dimensional notch radius $R' = R/(D/2)$. In a similar fashion, we refer to the dimensionless material dependent control radius $R'_1 = R_1/(D/2)$.

2.2. Analytical determination of the singularity-based control radius

Assuming a linear elastic material model and a perfectly sharp (zero radius) notch shown in Fig. 1 (b), the strain energy density SED is:

$$\overline{W}_1 = \frac{I_1}{4E(1-s)(\pi-\alpha)} \left(\frac{\sqrt{2\pi} K_N}{{R_1}^s} \right)^2 + \text{higher order terms} \tag{1}$$

Where I_1 is a non-dimensional parameter, which is a function of 2α and material Poisson's ratio ν and is determined from numerical analyses (reported below). The singular stress term approximation of Eq. 1 is initially considered:

$$\overline{W}_1 = \frac{I_1}{4E(1-s)(\pi-\alpha)} \left(\frac{\sqrt{2\pi} K_N}{{R_0}^s} \right)^2 \tag{2}$$

where R_0 is a first approximation of R_1 simply under the assumption of dominant singular stress term, and K_N is the NSIF[2] defined as:

$$\sigma_y(x) = \frac{K_N}{x^s} \tag{3}$$

[2]In the present paper, K_N is deprived of the constant factor $\sqrt{2\pi}$ unlike in other relevant literature [26].

where s is the power law singularity exponent[3], or degree of singularity according to Williams' analysis [44]. The dimensionless NSIF for unitary net stress and unitary length scale is defined as:

$$K_{\mathrm{N,UU}} = \frac{K_{\mathrm{N}}}{\sigma_{\mathrm{N}}(D/2)^s} \tag{4}$$

By combining Eq. 2 and 4, the average strain energy associated with the fatigue limit stress range is:

$$\Delta\overline{W}_1 = \frac{I_1}{4E(1-s)(\pi-\alpha)}\left(\frac{\sqrt{2\pi}K_{\mathrm{N,UU}}}{R_0'^{\,s}}\right)^2 \Delta\sigma_{\mathrm{N,fl}}^2 \tag{5}$$

where the singularity-based control radius is introduced in the dimensionless form $R_0' = R_0/(D/2)$ in agreement with the dimensionless radii previously introduced.

In the case of a plain sample under the same loading condition, the average SED is given by:

$$\Delta\overline{W}_{1,\mathrm{plain}} = \frac{1}{2E}\Delta\sigma_{\mathrm{fl}}^2 \tag{6}$$

By imposing the equality of Eq. 5 and 6, owing to an equally critical loading condition:

$$\frac{I_1}{4E(1-s)(\pi-\alpha)}\left(\frac{\sqrt{2\pi}K_{\mathrm{N,UU}}}{R_0'^{\,s}}\right)^2 \Delta\sigma_{\mathrm{N,fl}}^2 = \frac{1}{2E}\Delta\sigma_{\mathrm{fl}}^2 \tag{7}$$

Equation 7 can be inverted to obtain the singularity-based radius R_0':

$$R_0' = \left(\frac{K_{\mathrm{N,UU}}}{K_{\mathrm{f}}}\sqrt{\frac{\pi I_1}{(1-s)(\pi-\alpha)}}\right)^{1/s} \tag{8}$$

where $K_{\mathrm{f}} = \Delta\sigma_{\mathrm{fl}}/\Delta\sigma_{\mathrm{N,fl}}$ is the fatigue notch factor. Similar expressions have already been derived for R_0 (see for instance [20, 29]), however, Eq. 8 is formulated to emphasize the role of K_{f}.

In the present analysis, K_{f} is assumed to be known from fatigue experiments carried out on notched and plain specimens under the same load ratio. In principle, a single load ratio can be considered and the fatigue analyses extended to different load ratios by introducing the SED load ratio-dependency proposed in [24, 45]. However, this approach is not investigated here.

Although the singularity assumption underpinning Eq. 8 may lead to inconsistent estimations especially for large notch radiuses or short control radiuses, R_0' is regarded as the input of the inverse search procedure of the actual control radius R_1'. This requires finite element (FE) simulations to incorporate the effect of the actual radiused notch tip.

[3]Williams' eigenvalue λ_1 is usual in the literature, while its complement to 1, $s = 1-\lambda_1$, is introduced here for a simpler power law form.

3. Finite Element analysis

Table 1 lists the values of the parameters K_N and s, which control the singular stress state in the perfectly sharp notch (zero radius). They were calculated using the FE model devised in [27]. In that previous work, a very refined mesh close to the notch apex was used to accurately capture the theoretical power law singularity predicted by the Williams' analysis [44]. The strain energy density $\overline{W}_1$ was instead calculated using the axisymmetric FE model depicted in Fig. 2 (a), where the discretization of the critical volume of radius R_1 is obtained by creating a circular area in the FE model centred in the notch tip. It was thus possible to determine the SED directly from the subset of elements belonging to this area, thus limiting discretization errors as much as possible in the definition of the critical volume contour. The FE model employs quadratic 8-node elements PLANE183 available in ANSYS® element library.

For the V-notched geometry specifically investigated in the present paper, Eq. 1 fitted very well by reducing the higher order terms to just a constant. The coefficient I_1 can thus be determined. Its best-fit values are listed in Table 1 for the notch opening angle α and Poisson's ν values explored in the present paper.

Table 1: Coefficients for the singularity-based analysis of the V-notched specimen.

			I_1			m		
2α	s	$K_{N,UU}$	$\nu = 0.27$	$\nu = 0.30$	$\nu = 0.33$	$\nu = 0.27$	$\nu = 0.30$	$\nu = 0.33$
60°	0.487779	0.2866	0.84387	0.79271	0.73898	0.96829	0.97696	0.98745
90°	0.455516	0.3210	0.81715	0.77192	0.72467	0.97352	0.98043	0.98884

The FE model devised to estimate $\overline{W}_1$ in the critical volume at the tip of the rounded notch is shown in Fig. 2 (b). Also in this case, a circular arrangement of quadrilateral elements is used for an accurate representation of the critical volume contour. The mesh level refinement is the same as that used in the FE model of the perfectly sharp-notched specimen. The FE model was employed to build up a wide $\overline{W}_1$ database with the following notched sample configuration parameters:

$$R'_1 = \{0.0025, 0.005, 0.0075, 0.01, 0.015, 0.02, 0.03, 0.04, 0.05, 0.06, 0.07, 0.08\} \tag{9}$$

and the dimensionless notch radius:

$$R' = \{0.01, 0.02, 0.05, 0.075, 0.1, 0.15, 0.2\} \tag{10}$$

for all the combinations $2\alpha = \{60°, 90°\}$ and $\nu = \{0.27, 0.30, 0.33\}$.

This numerical database was used to calculate the inversion functions (explained in the next section), which were then analytically modelled to solve the inversion problem with a satisfactorily accurate approximation, without the need to repeat the specific FE analysis for any single radius ratio value.

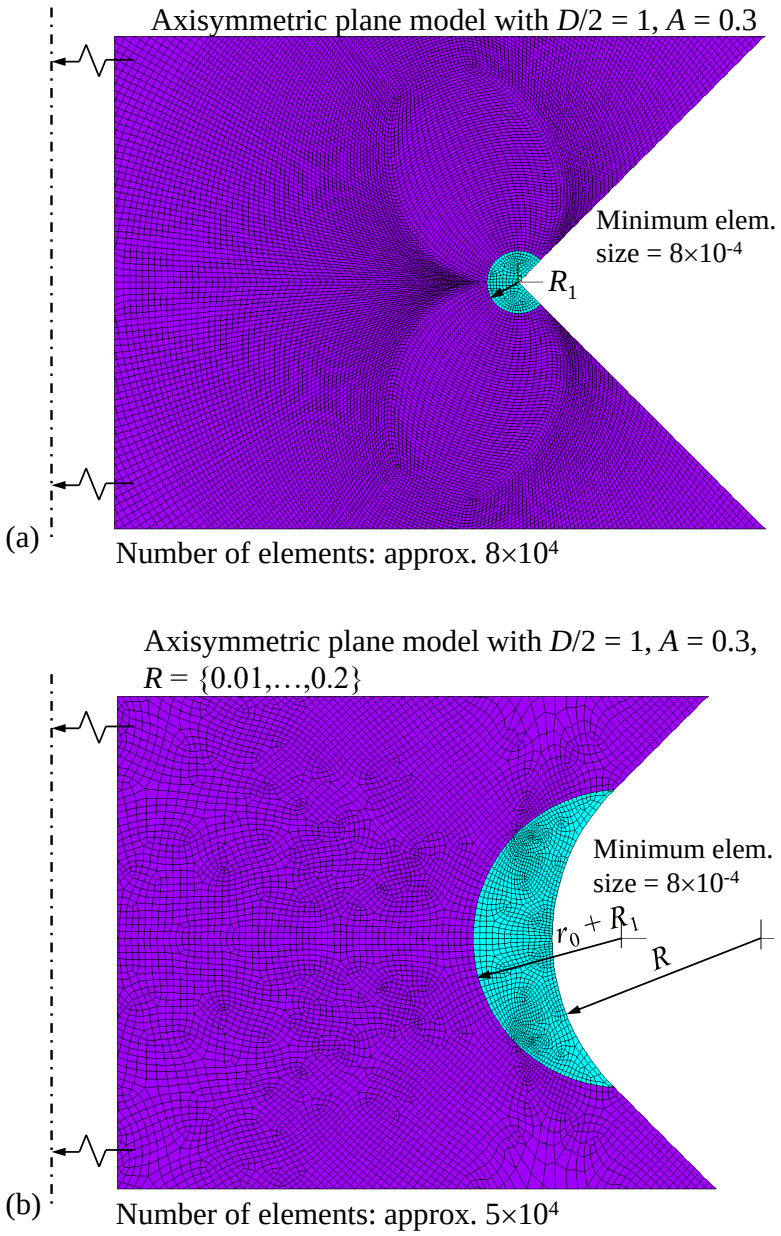

Figure 2: Parametric FE axisymmetric plane model of a perfectly sharp specimen (a) and a radiused specimen (b), where the lenticular area is created in the model geometry.

An analysis of the FE mesh sensitivity was performed for a single case used as a reference, namely $R' = 0.1$. A percentage relative deviation was calculated to obtain the order of magnitude of the numerical error:

$$\delta = 100\frac{\overline{W}_1 - \overline{W}_{1,\text{maxref}}}{\overline{W}_{1,\text{maxref}}} \tag{11}$$

where $\overline{W}_1$ is the SED calculated with any mesh level, while $\overline{W}_{1,\text{maxref}}$ is the SED obtained with the most refined explored mesh with a dimensionless element size $e/(D/2) = 3 \times 10^{-4}$.

As shown in Fig. 3, the relative deviation of the SED decreases with increasing size of the control radius. Moreover, being an energy-based evaluation, this deviation declines quite fast with respect to the element size.

The slope ratio is 3 to 1 in a log-log scale, or in other words δ is proportional to e^3. After this convergence analysis, the level of the mesh refinement was set to obtain $\overline{W}_1$ estimations in agreement with those published in [29] when the plane strain element behaviour is enforced, leading to a relative element size of 8×10^{-4}. This mesh resolution was then applied to the whole set of analyses, keeping the relative deviation below 10^{-4}% for all the explored control radius values. Accurate SED estimations were also obtained even with coarser meshes [14], consisting in a few tens of elements in the critical lenticular area. However, this refined mesh was implemented here to obtain an extremely accurate model aimed at setting the numerical values of the coefficients for the calculation procedure introduced below.

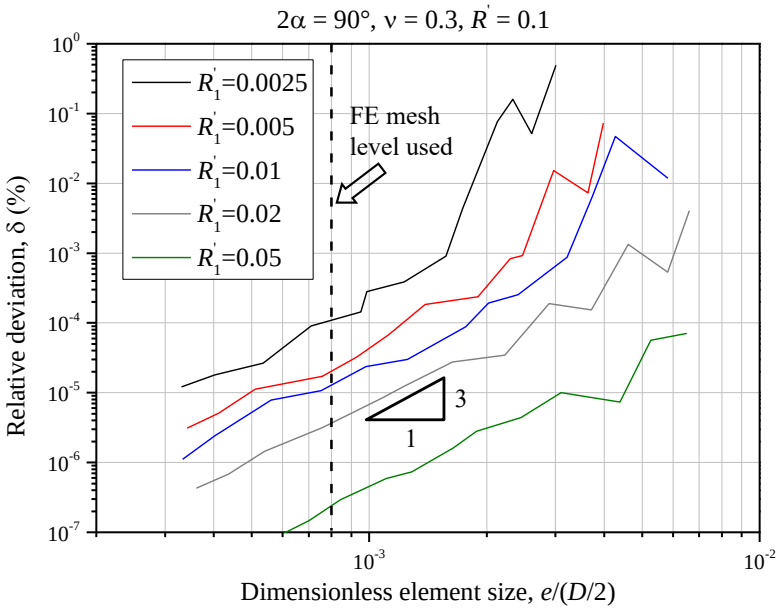

Figure 3: FE mesh convergence analysis of the SED, with respect to the relative element size, for various control radius values.

4. SED control radius inverse search

4.1. Procedure formulation of the inverse search

As evident from Eq. 1, the singular stress term is dominant only in the vicinity of the notch tip. Moving away from it, other higher order stress terms significantly contribute to $\overline{W}_1$. This effect is visible in Fig. 4, where the numerically estimated dimensionless control radius R'_1 progressively deviates from its first approximation R'_0 with the increasing control radius. Thus, the following simple linear relationship is proposed for calculating the actual value of R'_1 for the perfectly sharp V-notched specimen:

$$R'_1 = m(\alpha, \nu) R'_0 \tag{12}$$

where the angular coefficient m depends on α and ν and its best-fit estimation is listed in Table 1. Interestingly, m is quite close to unity, meaning that the effect of the higher order terms is almost negligible even for a relatively

large control radius size provided that the notch radius is (hypothetically) zero.

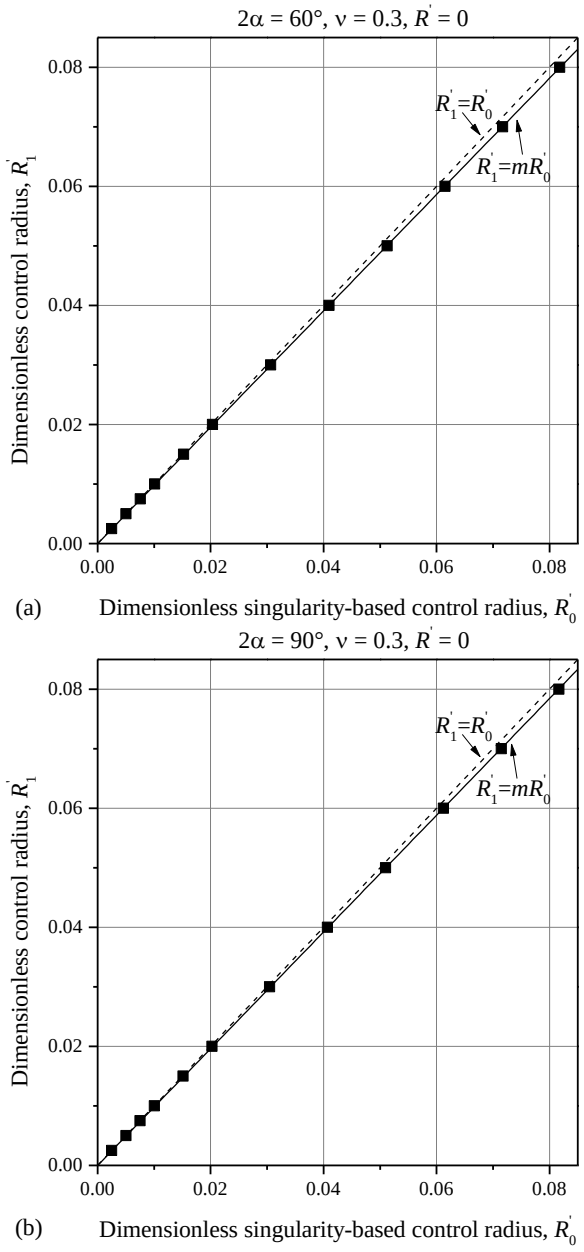

Figure 4: Linear dependency between the singularity-based control radius and the (actual) control radius for the perfectly sharp V-notch with opening angle $2\alpha = 60^\circ$ (a) and $2\alpha = 90^\circ$ (b).

When the control radius is estimated from $\overline{W}_1$ calculated for a rounded V-notched specimen, its singular stress-based estimation R'_0 must also be corrected for the effect of the notch radius. This situation is exemplified by Figs. 5 (a) and (b), which show the map (dotted values) of R'_1 vs. R'_0, parametric in R', for notch angles $2\alpha = 60^\circ$ and $2\alpha = 90^\circ$, respectively, and $\nu = 0.3$. It is evident that the relationship R'_1 vs. R'_0 gradually deviates from the linearity with increasing R'.

This non-linear dependency of R'_1 upon R'_0 is modelled here by proposing a summation of half-integer exponent

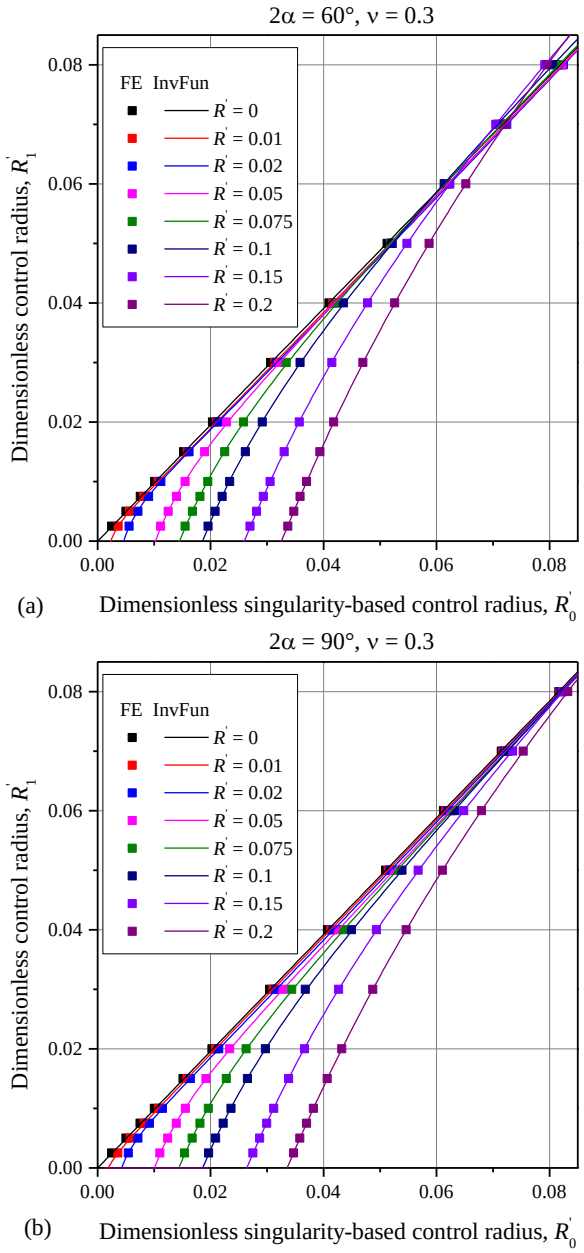

Figure 5: Dependency between the singularity-based control radius and the (actual) control radius for different radiused V-notches with opening angle $2\alpha = 60°$ (a) and $2\alpha = 90°$ (b).

terms, after the linear term previously introduced:

$$R'_1(\alpha,\nu,R') = m(\alpha,\nu)R'_0 + \sum_{i=1}^{4} a_i(\alpha,\nu,R')R'_0{}^{1-\frac{i}{2}} \tag{13}$$

where the functions $a_i(\alpha,\nu,R')$ are expected to tend to zero for vanishingly small R' and hence the perfectly sharp notch. Therefore, the following expression is proposed for modelling their dependency on R':

$$a_i(\alpha,\nu,R') = \sum_{j=1}^{5} b_{ij}(\alpha,\nu)R'^{\frac{j}{2}} \tag{14}$$

The entire calculation is in dimensionless form, and then, after Eq. 13, the physical size of the control radius can

be easily obtained:

$$R_1 = R_1' \frac{D}{2} \tag{15}$$

The constants b_{ij} were calculated separately for the explored values of α and ν by fitting the data corresponding to the conditions imposed by the FE analyses. In order to also keep the fitting accurate in the region of low R' values, the error variance to be minimized was normalized with respect to each data point. A reasonable compromise between the number of parameters needed to define the inversion function and the accuracy and stability in the numerical solution of Eqs. 13, 14 was obtained by assuming the maxima for the indexes i, j as 4 and 5, respectively.

The fitting capability of Eqs. 13, 14 is shown in Fig. 5 (solid curves). The relative error of the inverse function to predict the (actual) control radius R_1' is defined as:

$$\varepsilon = 100 \frac{R'_{1,\mathrm{InvFun}} - R'_{1,\mathrm{FE}}}{R'_{1,\mathrm{FE}}} \tag{16}$$

where the subscripts "InvFun" and "FE" obviously denote the value of the estimated control radius from the inverse function and the numerical model, respectively. ε is plotted in Figs. 6 (a) and (b) as a function of R_1' and R' for notch angles 2α equal to 60° and 90°, respectively, and $\nu = 0.3$. The error is very low (less than 1%) in large portions of the explored domain, except for R' values lower than 0.0075, where the absolute error increases up to about 5%. Nonetheless, such an error level is considered acceptable in this region, in view of the low values of $R'_{1,\mathrm{FE}}$ which greatly enhance the relative deviation of $R'_{1,\mathrm{InvFun}}$ from $R'_{1,\mathrm{FE}}$.

This procedure is considered reliable up to a relatively large control radius, such as $R_0' = 0.08$ for which the corresponding R_1' is quite similar for any notch radius, as shown in Fig. 5. On the other hand, the inversion procedure may return a value of R_1' close to zero for a small R_0', depending on the notch radius R'. The satisfaction of this limit condition can be expressed in terms of a minimum value for R_0', for which a summation expression is again proposed:

$$R'_{0,\min} = \sum_{k=1}^{3} c_k {R'}^{\frac{k+1}{2}} \tag{17}$$

where c_k are fitting coefficients tabulated in Appendix A. Whenever R_0' is larger than $R'_{0,\min}$, the output control radius R_1 is reliable and positive. On the other hand, when R_0' approaches $R'_{0,\min}$, the output result R_1 reduces to a vanishingly small value. Under this condition, the volume, within which the strain energy is averaged, is so small that the obtained SED equals the peak value achieved at the notch tip. In this situation, the corresponding fatigue notch factor K_f is the highest possible and obviously is equal to the (theoretical) stress concentration factor K_t of the notch. Figure 7 shows this minimum radius and the corresponding condition of the highest fatigue notch factor $K_{\mathrm{f,max}} = K_\mathrm{t}$ depending on the notch radius R' and for the two explored opening angles α.

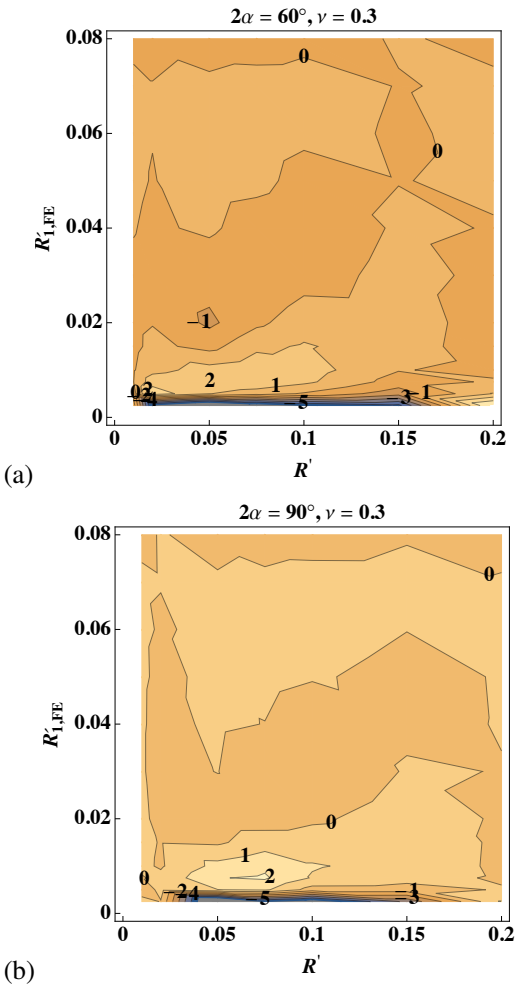

Figure 6: Percentage relative difference between the FE control radius and the inverse search procedure result for the opening angle $2\alpha = 60°$ (a) and $2\alpha = 90°$ (b).

4.2. Inverse search sensitivity

The proposed inverse search is considered valid in the R'_0 range of between the minimum $R'_{0,\min}$ and maximum value of 0.8. However, although performed in this range, the inverse search may be ill-posed whenever the control volume encloses a low gradient stress distribution. This situation occurs in two circumstances, i.e. (i) when the control radius R_1 is too small with respect to the notch radius R, or (ii) when R_1 is relatively large with respect to the external specimen radius $D/2$. If it is too small, the stress acting on the control volume is close to the peak value at the notch root. If it is larger, the average stress distribution is not affected by high gradient stress concentration produced by the notch. In order to identify the conditions of ill-posed inverse search, a sensitivity indicator S is defined as:

$$S = -\frac{1}{R_1}\frac{\mathrm{d}R_1}{\mathrm{d}K_\mathrm{f}} \tag{18}$$

Clearly, Eq. 18 expresses the sensitivity of the control radius to the uncertainty on the input of the inverse search,

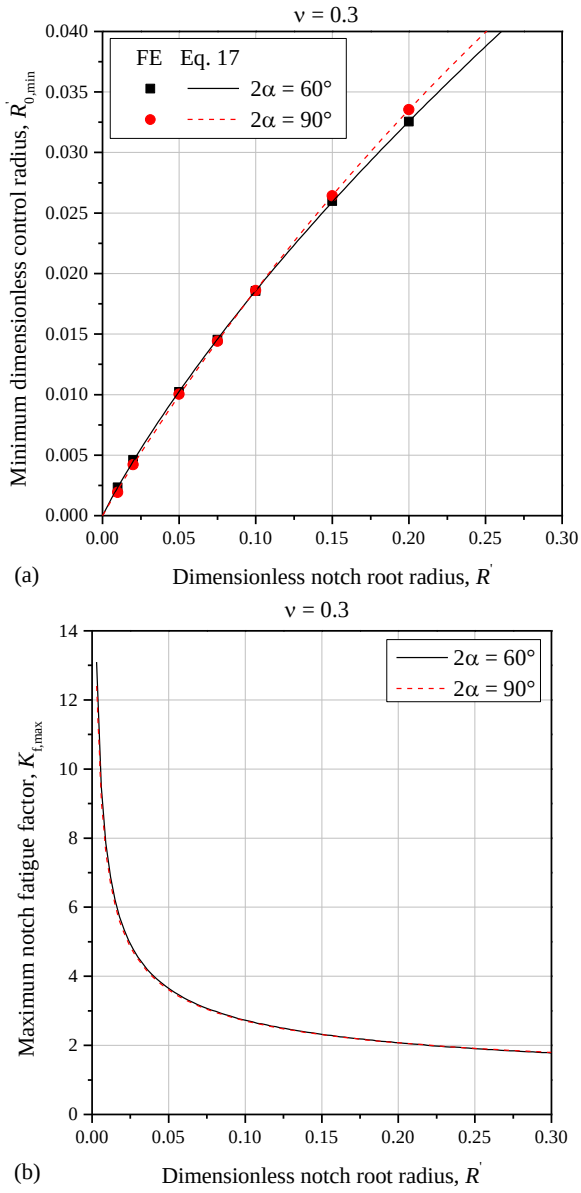

Figure 7: (a) Minimum singularity-based control radius leading to zero (actual) control radius. (b) Maximum fatigue notch factor corresponding to the minimum control radius.

i.e. the fatigue notch factor K_f. In Fig. 8, S exhibits a minimum at a certain value of R'_1, which depends on the notch radius. Performing the inverse search at R'_1 values that are far from this optimal value renders its estimation very sensitive to small deviations of the input K_f. Interestingly, the sharpest explored notch ($R' = 0.01$) sets a lower bound on the sensitivity parameter S, although for large values of the control radius, the notch radius increasingly plays a less important role. It might appear that the sharper the notch, the more accurate the R'_1 inverse search, but in fact the choice of the notch radius is not only dictated by accuracy, but also has to take into account manufacturing issues. The next section shows that satisfactory results are obtained with notch radius $R = 0.2$ mm and diameter $D = 20$ mm, or 7.7 mm for additively manufactured specimens, made of materials

with control radii of between 35 μm and 200 μm. However, in the case of materials with an even smaller control radius, a tooltip with a sharpness of $R = 0.1$ mm is recommended.

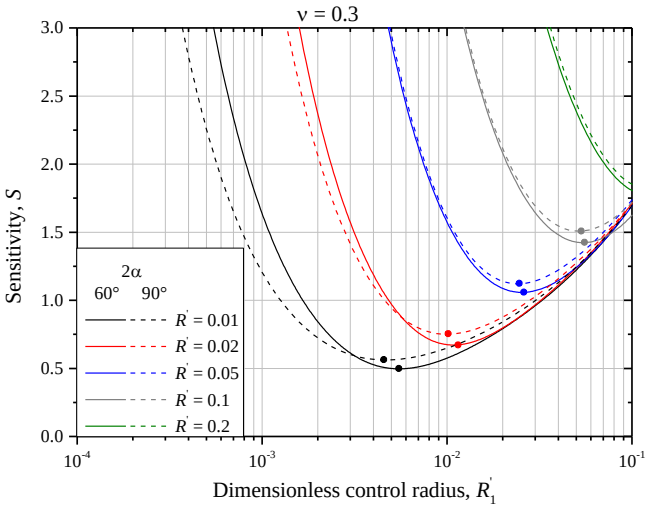

Figure 8: Sensitivity of the control radius inverse search with respect to the fatigue notch factor, for different opening angles and notch radii.

4.3. Inverse search procedure summary

The proposed inverse search procedure can be summarized in the following steps:

1. Experimentally obtain the fatigue limit of the plain and the V-notched specimen, the latter with a preferably sharp notch, and obtain the fatigue notch factor K_f;
2. Convert K_f into the singularity-based control radius R'_0 (Eq. 8), after introducing the correct values for the parameters $s, K_{N,UU}$ and I_1 listed in Table 1.
3. Verify that the obtained R'_0 is higher than the minimum allowed value $R'_{0,min}$ (Eq. 17).
4. Obtain R'_1 from Eq. 13, using the best-fit coefficients available in Appendix A;
5. Determine the (actual) control radius by multiplying R'_1 by the specimen external radius (Eq. 15).

This procedure is implemented in MATLAB® script files provided in the online version of this paper. Here, the dependence on Poisson's ratio ν is linearly interpolated for any value in the range $0.27 - 0.33$. The use of these scripts is briefly explained in Appendix B.

4.4. Notched specimen fatigue strength determination

The availability of a large and accurate set of numerical simulations is also exploited in order to derive an analytical procedure for determining the fatigue strength of the specimen, assuming the known material length R_1. In other words, the input and output variables of Fig. 5 are reversed with respect to the inverse search. This

task, referred herein to as *direct problem*, basically consists in the inversion of Eq. 13, which is here proposed through the following equation:

$$R'_0(\alpha,\nu,R') = \frac{R'_1}{m(\alpha,\nu)} + d_1(\alpha,\nu,R') + \sum_{i=2}^{4} d_i(\alpha,\nu,R') {R'_1}^{\frac{i}{2}} \tag{19}$$

where the notch radius dependency of the coefficients d_i is modelled as:

$$d_i(\alpha,\nu,R') = \sum_{j=1}^{5} e_{ij}(\alpha,\nu) {R'}^{\frac{j}{2}} \tag{20}$$

The e_{ij} values are available in Appendix A and the software implementation is provided and briefly explained in Appendix B. After the singularity-based R'_0 is found with Eq. 19, K_f is then obtained just by inverting Eq. 8:

$$K_\mathrm{f} = \frac{K_\mathrm{N,UU}}{{R'_0}^{s}} \sqrt{\frac{\pi I_1}{(1-s)(\pi-\alpha)}} \tag{21}$$

Finally, the fatigue limit stress amplitude of the notched specimen is obtained with the available K_f, provided that the plain fatigue limit is known.

5. Experimental result

The experimental data derived from our previous papers [40] and Benedetti and Santus [42] are reconsidered in this paper and then analysed with the proposed procedure. In [40], two common structural alloys, viz. the aluminium 7075-T6 and the steel 42CrMo4+QT, were tested under the load ratios $\mathrm{R} = -1$ and $\mathrm{R} = 0.1$. In [42], notched samples were additively manufactured by selective laser melting (SLM) of titanium alloy Ti-6Al-4V and fatigue tested at the load ratio $\mathrm{R} = -1$. To explore the effect of defectiveness on the notch fatigue strength, two sample batches were fabricated. The first one, termed T-N, is obtained by turning the notch from plain cylindrical bars, while in the second batch, termed SLM-N, the notch geometry is already introduced by the SLM process and a slight turning finish was applied to restore the correct notch radius.

Figure 9 summarizes the fatigue data used here to calculate the fatigue notch factor K_f, namely the S-N curves of the plain and sharp-notched (notch radius $R = 0.2$ mm) specimens. More precisely, the actual value of the plain fatigue strength of Ti-6Al-4V was calculated using the $\sqrt{area}$ Murakami model calibrated in [46] to account for the actual size of the critical defect leading to fatigue failure.

Using the procedure proposed in this work, as summarized in Section 4.3, the material control radius is calculated not only at the fatigue limit but also as a function of the number of cycles to failure N_f, by calculating K_f for any sampling of N_f. The experimentation undertaken in [40, 42] also included the measurement of the SIF threshold range ΔK_th. It was thus possible to estimate the threshold-based critical distance L_th according to the well-known formula:

$$L_\mathrm{th} = \frac{1}{\pi} \left(\frac{\Delta K_\mathrm{th}}{\Delta \sigma_\mathrm{fl}} \right)^2 \tag{22}$$

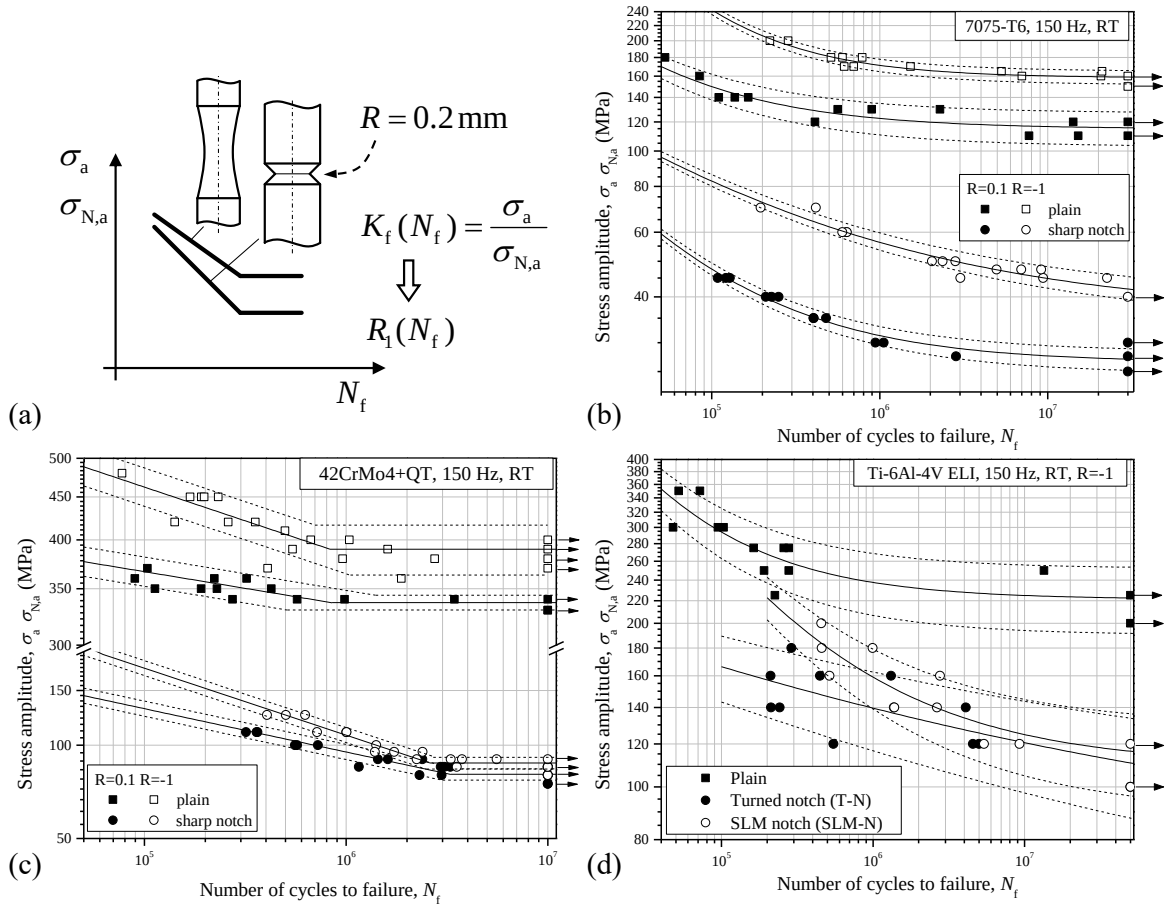

Figure 9: (a) Fatigue notch factor of a sharp V-notch for the control radius inverse search. Experimental data for the metal alloys (b) aluminium 7075-T6, (c) steel 42CrMo4+QT and (d) SLM titanium alloy Ti-6Al-4V.

whose outcomes are compared with the critical distance L obtained from the inverse search following the Line Method (LM) formulation of TCD.

Similarly, a threshold-based estimation of the control radius is also available in the literature, such as in [24], again by combining the crack threshold fatigue resistance and the plain specimen fatigue limit, or equivalently by rescaling L_{th} with a factor slightly lower than unity:

$$R_{1,\mathrm{th}} = \frac{(1+\nu)(5-8\nu)}{4} L_{\mathrm{th}} \tag{23}$$

These lengths are reported in Table 2 for all the investigated materials and loading conditions, taking the threshold-based values as a reference. For 7075-T6 and 42CrMo4+QT, a good correlation is found between the sharp specimen inverse search lengths and the threshold values, with a slight overestimation tendency affecting the SED method. On the other hand, as discussed in a previous work [42], the fracture mechanics tests performed for ΔK_{th} determination failed to capture the actual effect of defectiveness on both crack initiation and early propagation in the notched samples. As a consequence, notch-based estimations of both critical distance and control radius strongly deviated from the threshold-based ones. The fatigue calculation of the blunt-notched

samples in [42] turned out to be more accurate using sharp-notch derived lengths, instead of threshold-derived lengths.

Table 2: SED and LM inverse search and threshold-based lengths for the investigated aluminium alloy, steel and SLM titanium alloy.

Material	Experimental condition	Fat. life (cycles)	R_1 (mm)	$R_{1,\text{th}}$ (mm)	L (mm)	L_{th} (mm)
7075-T6	$R=-1$	30×10^6	0.0663	0.0436	0.0548	0.0555
	$R=0.1$		0.0390	0.0290	0.0327	0.0370
42CrMo4+QT	$R=-1$	10×10^6	0.0348	0.0366	0.0273	0.0433
	$R=0.1$		0.0483	0.0307	0.0367	0.0363
Ti-6Al-4V SLM	T-N, $R=-1$	50×10^6	0.1947	0.0258	0.1799	0.0304
	SLM-N, $R=-1$		0.1209	0.0158	0.1066	0.0187

A further interesting validation exercise consists in using the inverse search R_1 estimate to assess the fatigue strength of an independent batch of samples displaying the same cylindrical V-notched geometry, but carrying a blunter notch with radius $R = 1.0$ mm. The same fatigue calculation is also done with the threshold-derived control radius $R_{1,\text{th}}$ for comparison. The same approach is followed applying the LM formulation of the TCD. Despite a better correlation between the inverse search and the threshold-based values of the LM, the SED provides lower estimation errors of the blunt notch specimen fatigue strengths, also for the SLM titanium alloy, as shown in Table 3. The maximum errors obtained are well within the range of 10% and some are even lower than 1%.

Table 3: SED and LM evaluations of the blunt specimen fatigue limits for the investigated aluminium alloy, steel and SLM titanium alloy.

Material	Experimental condition	Fat. life (cycles)	Blunt (MPa)	SED, R_1 (MPa)	Err. (%)	SED, $R_{1,\text{th}}$ (MPa)	Err. (%)	LM (MPa)	Err. (%)
7075-T6	$R=-1$	30×10^6	62.3	64.0	2.8	62.4	0.2	61.8	-0.8
	$R=0.1$		45.0	45.2	0.4	44.6	-0.8	43.2	-4.0
42CrMo4+QT	$R=-1$	10×10^6	163	149	-8.5	150	-8.3	144	-12
	$R=0.1$		119	131	10	128	7.8	127	5.4
Ti-6Al-4V SLM	T-N, $R=-1$	50×10^6	117	123	5.4	102	-13	126	8.0
	SLM-N, $R=-1$		145	146	0.8	129	-11	146	0.8

It is also interesting that the fatigue predictions carried out with R_1 derived from the sharp notched geometry exhibit a comparable accuracy to those obtained from the threshold-derived control radius in the case of conventionally processed materials. On the other hand, for the SLM-manufactured Ti-6Al-4V, the accuracy of such estimations is considerably better with sharp-notch-derived R_1. This demonstrates that the method proposed in the present paper is also particularly suitable for fatigue calculations of additive materials. Besides a better fatigue strength estimation, the present method also avoids fracture mechanics tests which can be very challenging and expensive for this class of materials.

Following our previous work [40], this approach is extended to the finite life fatigue regime. Accordingly, the dependency of K_f upon the number of cycles to failure N_f is converted into a $R_1(N_f)$ function, which is plotted in Fig. 10 for all the material variants explored so far. It should be noted that this function tends to decrease with increasing fatigue life. This is not surprising because it is consistent with the growing notch sensitivity displayed by most materials at longer fatigue life. Nevertheless, this trend tends to saturate at low values of N_f for Al 7075-T6 and Ti-6Al-4V alloys tested at fully reversed axial loading ($R = -1$). Once the function $R_1(N_f)$ is known, the fatigue notch factor is estimated with the proposed direct problem procedure. The resulting predictions of the fatigue strength of the blunt-notched specimen variants are shown in Fig. 11. Once again, satisfactorily accurate predictions are obtained, even in the finite life fatigue regime.

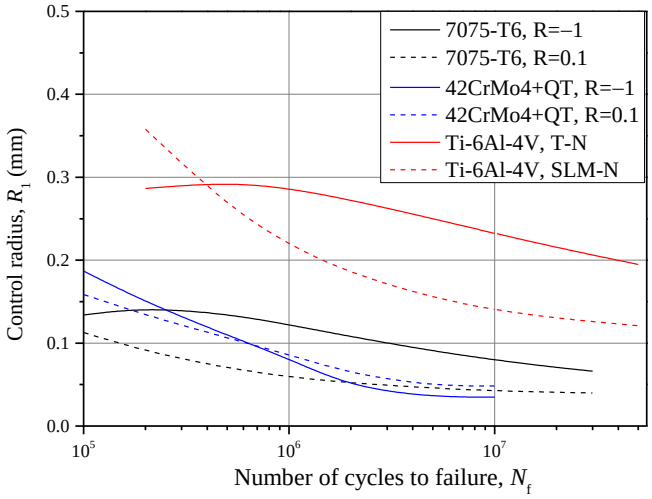

Figure 10: Control radius trends in the finite fatigue life regime for the investigated aluminium alloy, steel and SLM titanium alloy.

6. Conclusions

This paper has provided a complete procedure for the inverse search determination of the SED control radius. The reference specimen geometry is a V-notched bar with a sharp root radius, and the experimental input of the procedure is the fatigue stress concentration factor of this specimen. The calculation procedure was set in a dimensionless form, after considering one of the dimensions as a reference, viz. the external radius of the bar. A first estimate of the control radius was obtained from the hypothesis of the dominant singular stress term, similarly to other formulas already available in the literature based on the NSIF. However, this initial length turned out to be an accurate evaluation of the (actual) control radius only when it is quite large. On the other hand, when the control radius is small, which is a fairly common scenario for high strength metallic materials, the singularity-based radius is a large overestimation of the actual value. The availability of an accurate set of FE simulations led to the proposal of an analytical procedure that easily converts this singularity-based to the

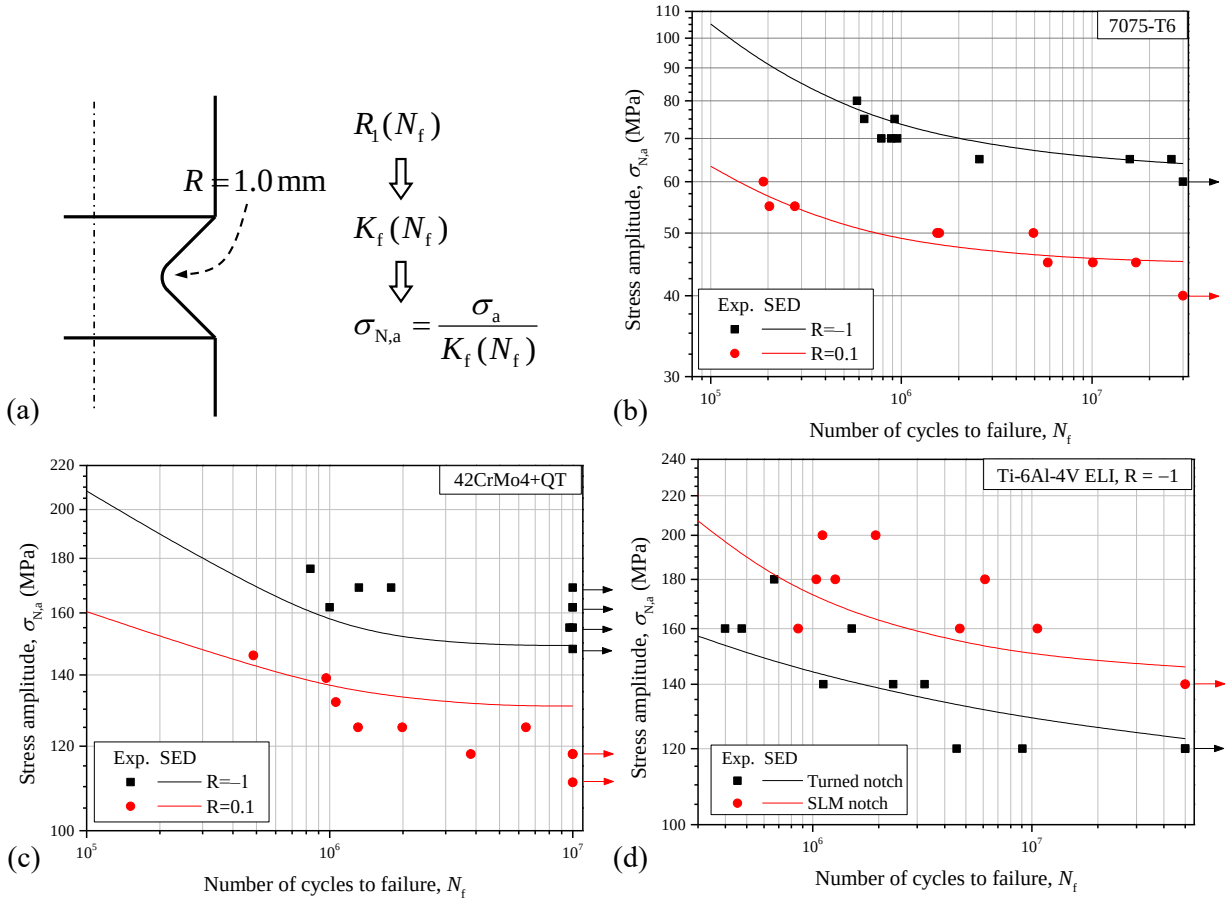

Figure 11: (a) Finite life fatigue strength assessment with the control radius function on the number of cycles to failure. Results and comparison with the experimental data for (b) aluminium alloy 7075-T6, (c) steel 42CrMo4+QT and (d) SLM titanium alloy Ti-6Al-4V.

(actual) control radius, without the need for any further FE calculation since formulas and the related coefficients are provided.

This procedure was subsequently applied to determine the control radius of three metallic materials at different load ratios. The radius values obtained were in the order of tens of microns, thus justifying both the correction from the singularity-based to the (actual) control radii, and the need for sharp notches to efficiently reduce the sensitivity to the experimental uncertainties. These lengths were compared with those obtained from the crack threshold stress intensity factor range. Similar length values were obtained for the traditional manufacturing materials, while for the additive manufacturing alloy, the threshold-based radii were significant larger than the V-notched specimen inverse search results found in this work. In addition, the fatigue strength of a blunter specimen was calculated, considering the inverse search determined lengths, and relative errors of a few percentage points were found compared with the experimental results, even for the additively manufactured alloy. The procedure was finally extended to the finite life regime, by calculating the fatigue notch factors at different numbers of cycles to failure. After the availability of the control radius at different numbers of cycles to failure, the fatigue

assessment was then repeated for the blunt notches and the finite life S-N curves were correctly reproduced.

References

[1] H. Neuber, Über die Berücksichtigung der Spannungskonzentration bei Festigkeitsberechnungen, Konstruktion 20 (1968) 245–251, in German.

[2] H. Neuber, Kerbspannungslehre, 3rd Edition, Springer-Verlag, Berlin, 1985, in German.

[3] S. D. Sheppard, Field effects in fatigue crack initiation: long life fatigue strength, Journal of Mechanical Design 113 (1991) 188–194.

[4] E. Beltrami, Sulle condizioni di resistenza dei corpi elastici, Tip. Bernardoni di C. Rebeschini, 1885, in Italian.

[5] G. C. Sih, Strain-energy-density factor applied to mixed mode crack problems, International Journal of Fracture 10 (1974) 305–321.

[6] L. F. Gillemot, Criterion of crack initiation and spreading, Engineering Fracture Mechanics 8 (1976) 239–253.

[7] P. Lazzarin, R. Zambardi, A finite-volume-energy based approach to predict the static and fatigue behavior of components with sharp V-shaped notches, International Journal of Fracture 112 (3) (2001) 275–298. doi:10.1023/A:1013595930617.

[8] P. Livieri, P. Lazzarin, Fatigue strength of steel and aluminium welded joints based on generalised stress intensity factors and local strain energy values, International Journal of Fracture 133 (3) (2005) 247–276. doi:10.1007/s10704-005-4043-3.

[9] C. Fischer, W. Fricke, C. M. Rizzo, Experiences and recommendations for numerical analyses of notch stress intensity factor and averaged strain energy density, Engineering Fracture Mechanics 165 (2016) 98–113. doi:10.1016/j.engfracmech.2016.08.012.

[10] C. Fischer, W. Fricke, C. M. Rizzo, Fatigue assessment of web-stiffened corners in plated structures by local approaches, Ship Technology Research 65 (2) (2018) 69–78. doi:10.1080/09377255.2018.1441781.

[11] D. Radaj, State-of-the-art review on the local strain energy density concept and its relation to the J -integral and peak stress method, Fatigue & Fracture of Engineering Materials & Structures 38 (1) (2015) 2–28. doi:10.1111/ffe.12231.

[12] G. Meneghetti, A. Campagnolo, F. Berto, Averaged strain energy density estimated rapidly from the singular peak stresses by FEM: Cracked bars under mixed-mode (I+III) loading, Engineering Fracture Mechanics 167 (2016) 20–33. doi:10.1016/j.engfracmech.2016.03.040.

[13] P. Lazzarin, F. Berto, Some Expressions for the Strain Energy in a Finite Volume Surrounding the Root of Blunt V-notches, International Journal of Fracture 135 (1-4) (2005) 161–185. doi:10.1007/s10704-005-3943-6.

[14] F. Berto, P. Lazzarin, Recent developments in brittle and quasi-brittle failure assessment of engineering materials by means of local approaches, Materials Science and Engineering: R: Reports 75 (2014) 1–48. doi:10.1016/j.mser.2013.11.001.

[15] A. R. Torabi, A. Campagnolo, F. Berto, Local strain energy density to predict mode II brittle fracture in Brazilian disk specimens weakened by V-notches with end holes, Materials & Design 69 (2015) 22–29. doi:10.1016/j.matdes.2014.12.037.

[16] A. R. Torabi, F. Berto, A. Campagnolo, J. Akbardoost, Averaged strain energy density criterion to predict ductile failure of U-notched Al 6061-T6 plates under mixed mode loading, Theoretical and Applied Fracture Mechanics 91 (2017) 86–93. doi:10.1016/j.tafmec.2017.04.010.

[17] M. R. Ayatollahi, A. R. Torabi, A. S. Rahimi, Brittle fracture assessment of engineering components in the presence of notches: a review, Fatigue & Fracture of Engineering Materials & Structures 39 (3) (2016) 267–291. doi:10.1111/ffe.12379.

[18] S. Cicero, F. Berto, F. T. Ibáñez-Gutiérrez, I. Procopio, V. Madrazo, SED criterion estimations of fracture loads in structural steels operating at lower shelf temperatures and containing u-notches, Theoretical and Applied Fracture Mechanics 90 (2017) 234–243. doi:10.1016/j.tafmec.2017.05.021.

[19] J. Justo, J. Castro, S. Cicero, Energy-based approach for fracture assessment of several rocks containing U-shaped notches through the application of the SED criterion, International Journal of Rock Mechanics and Mining Sciences 110 (2018) 306–315. doi:10.1016/j.ijrmms.2018.07.013.

[20] F. Berto, P. Lazzarin, J. R. Yates, Multiaxial fatigue of V-notched steel specimens: a non-conventional application of the local energy method, Fatigue & Fracture of Engineering Materials & Structures 34 (11) (2011) 921–943. doi:10.1111/j.1460-2695.2011.01585.x.

[21] F. Berto, P. Lazzarin, R. Tovo, Multiaxial fatigue strength of severely notched cast iron specimens, International Journal of Fatigue 67 (2014) 15–27. doi:10.1016/j.ijfatigue.2014.01.013.

[22] F. Berto, A. Campagnolo, P. Lazzarin, Fatigue strength of severely notched specimens made of Ti-6Al-4V under multiaxial loading, Fatigue & Fracture of Engineering Materials & Structures 38 (5) (2015) 503–517. doi:10.1111/ffe.12272.

[23] S. Vantadori, A. Carpinteri, G. Fortese, C. Ronchei, D. Scorza, A. Zanichelli, Fatigue lifetime evaluation of notched components: Implementation of the control volume concept in a strain-based LCF criterion, Theoretical and Applied Fracture Mechanics 97 (2018) 400–408. doi:10.1016/j.tafmec.2017.07.001.

[24] A. Campagnolo, G. Meneghetti, F. Berto, K. Tanaka, Crack initiation life in notched steel bars under torsional fatigue: Synthesis based on the averaged strain energy density approach, International Journal of Fatigue 100 (2017) 563–574. doi:10.1016/j.ijfatigue.2016.12.022.

[25] M. Peron, S. M. J. Razavi, F. Berto, J. Torgersen, L. Marsavina, Local strain energy density for the fracture assessment of polyurethane specimens weakened by notches of different shape, Frattura ed Integrità Strutturale 11 (42) (2017) 214–222. doi:10.3221/IGF-ESIS.42.23.

[26] F. Berto, S. M. J. Razavi, J. Torgersen, Frontiers of fracture and fatigue: Some recent applications of the local strain energy density, Frattura ed Integrita Strutturale 12 (43) (2018) 1–32. doi:10.3221/IGF-ESIS.43.01.

[27] C. Santus, D. Taylor, M. Benedetti, Determination of the fatigue critical distance according to the Line and the Point Methods with rounded V-notched specimen, International Journal of Fatigue 106 (2018) 208–218. doi:10.1016/j.ijfatigue.2017.10.002.

[28] ASTM, Standard Test Method for Measurement of Fatigue Crack Growth Rates, ASTM E647 – 15 (2015). doi:10.1520/E0647-15.
[29] F. Berto, P. Lazzarin, A review of the volume-based strain energy density approach applied to V-notches and welded structures, Theoretical and Applied Fracture Mechanics 52 (3) (2009) 183–194. doi:10.1016/j.tafmec.2009.10.001.
[30] D. Taylor, The Theory of Critical Distances: A New Perspective in Fracture Mechanics, Elsevier Science, 2007.
[31] L. Susmel, A unifying approach to estimate the high-cycle fatigue strength of notched components subjected to both uniaxial and multiaxial cyclic loadings, Fatigue & Fracture of Engineering Materials & Structures 27 (5) (2004) 391–411. doi:10.1111/j.1460-2695.2004.00759.x.
[32] X.-Y. Liu, T.-X. Su, Y. Zhang, M.-N. Yuan, A multiaxial high-cycle fatigue life evaluation model for notched structural components, International Journal of Fatigue 80 (2015) 443–448. doi:10.1016/j.ijfatigue.2015.07.010.
[33] M. Benedetti, V. Fontanari, M. Allahkarami, J. C. Hanan, M. Bandini, On the combination of the critical distance theory with a multiaxial fatigue criterion for predicting the fatigue strength of notched and plain shot-peened parts, International Journal of Fatigue 93 (2016) 133–147. doi:10.1016/j.ijfatigue.2016.08.015.
[34] L. Susmel, D. Taylor, The Theory of Critical Distances as an alternative experimental strategy for the determination of KIc and ΔKth, Engineering Fracture Mechanics 77 (9) (2010) 1492–1501. doi:10.1016/j.engfracmech.2010.04.016.
[35] D. Taylor, Applications of the theory of critical distances in failure analysis, Engineering Failure Analysis 18 (2) (2011) 543–549. doi:10.1016/j.engfailanal.2010.07.002.
[36] S. Cicero, V. Madrazo, I. A. Carrascal, On the Point Method load-bearing capacity predictions in Al7075-T651 structural components containing stress risers, Engineering Failure Analysis 26 (2012) 129–138. doi:10.1016/j.engfailanal.2012.07.008.
[37] L. Susmel, D. Taylor, The Theory of Critical Distances to estimate finite lifetime of notched components subjected to constant and variable amplitude torsional loading, Engineering Fracture Mechanics 98 (2013) 64–79. doi:10.1016/j.engfracmech.2012.12.007.
[38] T. Yin, A. Tyas, O. Plekhov, A. Terekhina, L. Susmel, A novel reformulation of the Theory of Critical Distances to design notched metals against dynamic loading, Materials & Design 69 (2015) 197–212. doi:10.1016/j.matdes.2014.12.026.
[39] W. Li, L. Susmel, H. Askes, F. Liao, T. Zhou, Assessing the integrity of steel structural components with stress raisers using the Theory of Critical Distances, Engineering Failure Analysis 70 (2016) 73–89. doi:10.1016/j.engfailanal.2016.07.007.
[40] C. Santus, D. Taylor, M. Benedetti, Experimental determination and sensitivity analysis of the fatigue critical distance obtained with rounded V-notched specimens, International Journal of Fatigue 113 (2018) 113–125. doi:10.1016/j.ijfatigue.2018.03.037.
[41] M. Benedetti, C. Santus, Mean stress and plasticity effect prediction on notch fatigue and crack growth threshold, combining the theory of critical distances and multiaxial fatigue criteria, Fatigue & Fracture of Engineering Materials & Structures-doi:10.1111/ffe.12910.
[42] M. Benedetti, C. Santus, Notch fatigue and crack growth resistance of Ti-6Al-4V ELI additively manufactured via selective laser melting: A critical distance approach to defect sensitivity, International Journal of Fatigue 121 (2019) 281–292. doi:10.1016/j.ijfatigue.2018.12.020.
[43] A. Campagnolo, F. Berto, D. Leguillon, Fracture assessment of sharp V-notched components under Mode II loading: a comparison among some recent criteria, Theoretical and Applied Fracture Mechanics 85 (2016) 217–226. doi:10.1016/j.tafmec.2016.02.001.
[44] M. L. Williams, Stress Singularities Resulting From Various Boundary Conditions in Angular Corners of Plates in Extension, Journal of Applied Mechanics, Transactions ASME 19 (1952) 526–528.
[45] A. A. Roostaei, A. Pahlevanpour, S. B. Behravesh, H. Jahed, On the definition of elastic strain energy density in fatigue modelling, International Journal of Fatigue 121 (2019) 237–242. doi:10.1016/j.ijfatigue.2018.12.011.
[46] M. Benedetti, V. Fontanari, M. Bandini, F. Zanini, S. Carmignato, Low- and high-cycle fatigue resistance of Ti-6Al-4V ELI additively manufactured via selective laser melting: Mean stress and defect sensitivity, International Journal of Fatigue 107 (2018) 96–109. doi:10.1016/j.ijfatigue.2017.10.021.

Appendix A. Procedure coefficients

All the coefficients required for implementing the introduced analytical procedure are listed in Tables A.4 and A.5 for the angles $2\alpha = 60^\circ$ and 90°, respectively.

Table A.4: Procedure coefficients b_{ij}, c_k, e_{ij} for the V-notch opening angle $2\alpha = 60^\circ$.

b_{ij}, $2\alpha = 60°$, $\nu = 0.27$				
-0.989328073890058	17.813823259543	-90.6045294353268	167.083764905978	-117.34355877894
0.430337393926397	-7.34850552179526	31.7888499557811	-44.6643542732263	30.8978160181794
-0.0468874403409467	0.671406233547507	-1.63282475196792	-0.362402021903228	-1.71271718687741
0.00119153032984861	-0.0113539021985702	-0.0265023762246038	0.0112690523663061	0.454074772025857

b_{ij}, $2\alpha = 60°$, $\nu = 0.30$				
-0.87283446134295	16.8978997736763	-86.8101955026814	159.828248496854	-111.574385495565
0.385355744945926	-6.99875540828892	30.4926412546144	-42.382217645198	28.7637874279468
-0.0427385260722818	0.64819600521387	-1.57373365840563	-0.482986790938427	-1.37252407496186
0.00107636656039123	-0.0108117536409329	-0.0297089849080886	0.0363224095344592	0.39418629794571

b_{ij}, $2\alpha = 60°$, $\nu = 0.33$				
-0.728516039061163	15.7174063589923	-81.7226309689693	149.730096019465	-103.412203934151
0.329848724648284	-6.54074146333182	28.6741236919471	-38.9614453456706	25.6257473658322
-0.0375555755844178	0.614111819673587	-1.46099831021301	-0.727351703200745	-0.898617670991334
0.000929765257390919	-0.00989916194211657	-0.0350094151730919	0.0677746123884689	0.325145721855587

c_k, $2\alpha = 60°$, $\nu = 0.27$	c_k, $2\alpha = 60°$, $\nu = 0.30$	c_k, $2\alpha = 60°$, $\nu = 0.33$
0.265134136101911	0.262500424215411	0.258817753859912
-0.261794753729463	-0.289834929851446	-0.316736433251523
0.10450087830991	0.149888820760047	0.194126870328609

e_{ij}, $2\alpha = 60°$, $\nu = 0.27$				
-0.0416895043994533	0.534232276092262	-0.0494437574758084	-3.31303452309238	4.61835259726765
16.5381709506653	-260.951075507378	1051.027425105	-1532.89306041663	643.126899620553
-132.938634414104	2219.69455130166	-10173.7195869152	17720.4072681687	-10253.6397183776
271.055900450231	-4679.64487586133	22956.8687207434	-43476.6520361241	28111.0730753127

e_{ij}, $2\alpha = 60°$, $\nu = 0.30$				
-0.0430836919523989	0.545139856322282	-0.146238088293208	-3.0796220954005	4.42436849222261
17.0615365769642	-269.273435994047	1096.12509417984	-1635.46647851813	726.709215102388
-135.057301929272	2262.73469359385	-10435.1992401458	18355.0291626082	-10792.7507975045
271.536321713192	-4724.49890228105	23298.5378743538	-44392.525390535	28935.3329052977

e_{ij}, $2\alpha = 60°$, $\nu = 0.33$				
-0.0448085647732817	0.560503799078809	-0.272530340725184	-2.77733467812804	4.17373992175202
17.6653179747844	-279.038885539751	1149.78821598411	-1758.85473223915	828.110685259756
-137.386492970239	2311.58113245602	-10737.825130363	19099.9835771169	-11432.3571116451
271.684841743297	-4771.74727357148	23678.0588140766	-45435.6850068412	29889.2534162476

Appendix B. Software implementation

The presented analytical procedure is available in the online page of this article, implemented in MATLAB® software. The script `RunThisFirst_SaveCoeffs.m` initially needs to be run in order to have all the coefficients introduced in the Workspace and saved in the file `Coeffs.mat`. A single inverse search example can then be performed with `InverseSearchExample.m`, and a direct problem solution is obtained with `DirectProblemExample.m`.

Table A.5: Procedure coefficients b_{ij}, c_k, e_{ij} for the V-notch opening angle $2\alpha = 90°$.

b_{ij}, $2\alpha = 90°$, $\nu = 0.27$				
-0.376359300730234	2.80423481800958	16.5733974171492	-109.236493392478	117.267715685101
0.0572266582288851	1.15430978025432	-25.1547912501891	93.144730551597	-79.2257315055048
0.0169891442941251	-0.670502780260079	6.64603805620584	-18.5707062827863	11.2786220100755
-0.00151772076610742	0.0407083507759149	-0.305863177012631	0.488127287539394	0.248828150035615

b_{ij}, $2\alpha = 90°$, $\nu = 0.30$				
-0.268743085230572	1.94556889988516	20.1063458905297	-115.140236702385	120.90408273904
0.0208700098248675	1.37133181190868	-25.5948971949987	92.8167813463111	-78.552034696077
0.0191496799637444	-0.657520284942311	6.46382320659689	-18.0087960827492	10.9383184467225
-0.00150734918788065	0.0388636834882311	-0.293561156013399	0.471225507632612	0.229996613104836

b_{ij}, $2\alpha = 90°$, $\nu = 0.33$				
-0.139467684276113	0.902066505962442	24.4589965489101	-122.596718788648	125.631061764697
-0.0227270138065701	1.64440117839016	-26.2366575338536	92.7770586562887	-78.0581679292328
0.0218407438571512	-0.646569160549642	6.28008454395666	-17.427586460807	10.5948996323297
-0.00150598862030264	0.0369788612852952	-0.280846967981236	0.454374278628544	0.208188545373248

c_k, $2\alpha = 90°$, $\nu = 0.27$	c_k, $2\alpha = 90°$, $\nu = 0.30$	c_k, $2\alpha = 90°$, $\nu = 0.33$
0.219126412959821	0.225983042762168	0.228572428718877
-0.0387177854891394	-0.114032072009441	-0.169118695153874
-0.142757126221946	-0.0367840192024039	0.0417809496552524

e_{ij}, $2\alpha = 90°$, $\nu = 0.27$				
-0.00639331868354599	-0.0332676581570811	2.80770557146795	-9.10074764311521	8.78323692224837
5.22393927709138	-60.7821379432436	-60.8521714060971	944.58816037681	-1290.10126975743
-47.7987965258794	651.380764869994	-1126.48888522558	-3070.89060158372	6398.95456460855
106.304076126221	-1554.96552094411	4427.25628864608	116.521872953601	-7509.33743595847

e_{ij}, $2\alpha = 90°$, $\nu = 0.30$				
-0.0070045948493102	-0.0327183466121512	2.76975491455637	-9.00162012082668	8.69610248579601
5.53293824234513	-65.1962182820118	-38.0190749949739	893.02211858674	-1247.67587644689
-48.7589765769744	671.082191282825	-1246.25164708423	-2774.72970760353	6140.75341147178
105.364998519936	-1565.97896514951	4547.8758459169	-249.206834607119	-7153.92026916731

e_{ij}, $2\alpha = 90°$, $\nu = 0.33$				
-0.00785029859546399	-0.0292692515212235	2.71265242796854	-8.85930671824068	8.57426172642451
5.92018003202763	-70.8607597319997	-8.21139706652348	825.149878463996	-1191.66643867236
-50.0349643905806	697.065555222776	-1405.32789362084	-2380.00325538247	5796.58043356604
104.500835982616	-1583.38989772708	4719.54905724912	-757.51818711554	-6666.12596688636

The data of the inverse search case of the (editable) script file is reported below:

$$2\alpha = 90^\circ, \quad \nu = 0.3, \quad D = 20\,\text{mm}, \quad R = 0.2\,\text{mm}, \quad K_\text{f} = 3.5 \tag{B.1}$$

which produces the result:

$$R_1 = 0.090721\,\text{mm} \tag{B.2}$$

As a validation example, the same lengths are introduced as input as for the direct problem:

$$2\alpha = 90^\circ, \quad \nu = 0.3, \quad D = 20\,\text{mm}, \quad R = 0.2\,\text{mm}, \quad R_1 = 0.090721\,\text{mm} \tag{B.3}$$

and the K_f result obtained is:

$$K_\text{f} = 3.4679 \tag{B.4}$$

with an error slightly lower than 1% with respect to the initial input $K_\text{f} = 3.5$.